

# Parsimonious Evaluation of Concentric-Tube Continuum Robot Equilibrium Conformation

Daniel Caleb Rucker\*, *Member, IEEE*, and Robert J. Webster III, *Member, IEEE*

**Abstract**—Dexterous at small diameters, continuum robots consisting of precurved concentric tubes are well-suited for minimally invasive surgery. These active cannulas are actuated by relative translations and rotations applied at the tube bases, which create bending via elastic tube interaction. An accurate kinematic model of cannula shape is required for applications in surgical and other settings. Previous models are limited to circular tube precurvatures, and neglect torsional deformation in curved sections. Recent generalizations account for arbitrary tube preshaping and bending and torsion throughout the cannula, providing differential equations that define cannula shape. In this paper, we show how to simplify these equations using Frenet–Serret frames. An advantage of this approach is the interpretation of torsional components of the preset tube shapes as “forcing functions” on the cannula’s differential equations. We also elucidate a process for numerically solving the differential equations, and use it to produce simulations illustrating the implications of torsional deformation and helical tube shapes.

**Index Terms**—Active cannula, continuum robot, medical robot, snake-like robot.

## I. INTRODUCTION

ELASTIC backbones give continuum robots “tentacle-like” dexterity, thus allowing them to maneuver through complex environments and winding passages. The active cannula is one type of continuum robot that is particularly useful in medicine because of its small diameter. Active cannulas consist of concentric, preshaped elastic tubes [2], which can be rotated and translated axially at their respective bases to transmit moments, creating bending (see Fig. 1). In minimally invasive surgery, this allows steering and aiming of surgical tools (e.g., fiber optic lasers, injectable drugs or thermal treatments, miniature surgical grippers, etc.) delivered through the central working channel of the innermost cannula tube. Using the cannula to accurately deliver these tools requires an accurate kinematic model of cannula shape in terms of individual tube preshaping and tube base positions.

In the past few years, models of active cannula shape have continually increased in generality and predictive power. All early work considered only circularly precurved tubes. The simplest model treats each outer tube as infinitely rigid (in both bending and torsion) compared to all those within it [3].

Manuscript received February 1, 2009; revised May 5, 2009. First published June 16, 2009; current version published August 14, 2009. Some results in this paper have been presented at the 2009 IEEE International Conference on Robotics and Automation [1]. This material is based upon work supported by the National Science Foundation under Grant No. 0651803. *Asterisk indicates corresponding author.*

\*D. C. Rucker is with the Vanderbilt University, Nashville, TN 37235 USA (e-mail: daniel.c.rucker@vanderbilt.edu).

R. J. Webster III is with the Vanderbilt University, Nashville, TN 37235 USA (e-mail: robert.webster@vanderbilt.edu).

Color versions of one or more of the figures in this paper are available online at <http://ieeexplore.ieee.org>.

Digital Object Identifier 10.1109/TBME.2009.2025135



Fig. 1. Prototype active cannula made of three superelastic nitinol tubes and one central wire.

This reduces cannula forward kinematics to the geometric problem of describing transformations along a piecewise circular robot, which can be solved in a number of ways (see, e.g., [4] for a Denavit–Hartenberg (DH) parameter approach). Subsequent experiments showed significant elastic interactions between tubes in the cannula backbone, and this effect was modeled via Bernoulli–Euler beam mechanics [5]–[7]. Torsion also strongly affects cannula shape, although it is more challenging to model and was initially approached in a limited sense (in the initial straight sections) [2]. Further work showed significant accuracy enhancements from including torsion in curved sections [8], [9] and enabled general precurved tube shapes to be used [9], significantly expanding active cannula capabilities.

### A. Contribution

In this paper, we build upon the model in [9], using the Frenet–Serret convention to reformulate the system of differential equations, thus yielding a concise form amenable to numerical integration. Furthermore, we explore model implications through simulations of multitube active cannulas and those with noncircular (helical) preset tube shapes, which have been beyond the scope of prior models.

## II. REVIEW OF KINEMATIC MODEL

In this section, for reader convenience, we provide a brief review of the active cannula forward kinematic model derived in [9], which is an extension of the framework given in [2]. The only difference between the formulation given in this section and that of [9] is the use of the Frenet–Serret frame convention to describe tube preshapes rather than rotation minimizing frames. The basic strategy employed is minimization of the total elastic energy stored in a collection of  $n$  preshaped elastic tubes to determine the equilibrium conformation (i.e., the shape of the overall cannula). This strategy has been applied to other continuum robot designs in the past, and further discussion of the elastic energy integral for a single rod can be found in [10]. In this paper, we use the well-known kinetic analogy [11], so that our equations are cast in the form of kinetics. For a review of the relationship of these symbols to equivalent mechanics symbols, see [11].

Following the assumptions common to all prior work, in this paper, we continue to neglect the effects of friction and gravity. Note that gravity in particular has little effect at the scale and stiffness of interest in an active cannula; gravity would cause only 60  $\mu\text{m}$  of tip deflection for a straight cantilevered tube 100 mm long with an OD of 1.6 mm, an ID of 1.3 mm, and a Young's modulus of 50 GPa.

Let each preset tube shape be defined by a curve through space  $p_i^*(s)$ , where  $s \in [0, \ell]$  is the arc length. We define a Frenet–Serret coordinate frame at each point along the curve of each pre-shaped tube in its undeformed state  $g_i^*(s) = \{R_i^*(s), p_i^*(s)\} \in \text{SE}(3)$ . Note here that alternate frame choices are possible, since energy is invariant to frame choice [9], but use of Frenet–Serret enables the final modeling result to be expressed in a convenient form, as will become clear shortly. The body frame “angular velocity” vectors (with respect to arc length rather than time) of the undeformed curves are then given by  $\omega_i^*(s) = (R_i^{*T}(s)\dot{R}_i^*(s))^\vee = \kappa_i(s)e_1 + \tau_i(s)e_3$ , where  $\kappa_i$  and  $\tau_i$  are the geometric curvature and torsion intrinsic to each undeformed tube centerline in the standard Frenet–Serret sense, and  $e_1, e_2, e_3 \in \mathbb{R}^3$  are the standard basis vectors.<sup>1</sup> As set forth in [12], the  $^\vee$  operator maps an element of the Lie algebras  $\mathfrak{se}(3)$  or  $\mathfrak{so}(3)$ , to the corresponding  $\mathbb{R}^6$  or  $\mathbb{R}^3$  element, respectively. The  $\hat{\cdot}$  operator denotes the inverse operation.

Now consider an arbitrary deformation of the  $i$ th tube consisting of bending and torsion with negligible shear and elongation. Such a deformation can be captured by a change in the angular velocity vector  $\Delta\omega_i(s)$ , so that the deformed tube angular velocity is described by  $\omega_i(s) = \omega_i^*(s) + \Delta\omega_i(s)$ . The deformed, framed curve  $g_i(s) = \{R_i(s), p_i(s)\} \in \text{SE}(3)$  is then defined by  $[e_3^T \ \omega_i^T]^T = (g_i^{-1}(s)\dot{g}_i(s))^\vee$ . Since these frames are defined by the deformation, in general, they will not correspond to the Frenet–Serret frames of the deformed shape.

The total elastic energy stored in these  $n$  deformed tubes is then the sum of the individual bending and torsional energy stored in each [2], [9], [10], [13]

$$E = \sum_{i=1}^n \underbrace{\frac{1}{2} \int_0^\ell \Delta\omega_i^T(s) K_i(s) \Delta\omega_i(s) ds}_{i\text{th tube energy}} \quad (1)$$

where  $K_i(s) = \text{diag}\{k_{i1}(s), k_{i2}(s), k_{i3}(s)\}$ . In this paper, we consider cylindrical tubes of constant moment of inertia  $I$  and polar moment  $J$ . In this case,  $k_{i1}(s) = k_{i2}(s) = E_i I_i$  and  $k_{i3}(s) = G_i J_i$ , where  $E$  denotes the elastic modulus and  $G$  the shear modulus. The active cannula shape will be such that this stored elastic energy is minimized [2], [10].

When the tubes are concentrically constrained, all  $R_i(s)$  share a common tangent  $e_3$  axis. Without loss of generality, we let the  $n$ th tube frame be a reference and parameterize the other frames by a rotation about  $e_3$ ,  $R_i(s) = R_n(s) \exp\{\hat{e}_3 \theta_i(s)\}$ , for  $i = 1, \dots, n$ . Therefore,

$$\omega_i(s) = (R_i^T \dot{R}_i)^\vee = e^{-\hat{e}_3 \theta_i(s)} \omega_n(s) + \dot{\theta}_i(s) e_3 \quad (2)$$

for  $i = 1, \dots, n$ . Substituting (2) into (1), and letting  $\omega = \omega_n$ , we rewrite (2) in a form that facilitates minimization. This is

<sup>1</sup>Consistent with prior active cannula frame conventions, frames are assigned to the undeformed curves such that the  $e_3$  axis is tangent to the curve, and positive curvature is about the  $e_1$  axis. This implies that the Frenet–Serret normal, binormal, and tangent correspond to  $-e_2, e_1$ , and  $e_3$ , respectively.

done by completing the square, and recognizing that  $K_i$  is diagonal with its first two elements equal. See [9] for an expanded discussion of the algebraic steps. This yields

$$E = \frac{1}{2} \int_0^\ell (\omega - \alpha)^T K (\omega - \alpha) + C ds \quad (3)$$

where

$$\alpha = K^{-1} \left( \sum_{i=1}^n K_i \bar{\omega}_i^* \right), \quad K = \sum_{i=1}^n K_i$$

$$\bar{\omega}_i^* = e^{\hat{e}_3 \theta_i} \omega_i^* - \dot{\theta}_i e_3,$$

and

$$C = \sum_{i=1}^n \bar{\omega}_i^{*T} K_i \bar{\omega}_i^* - \alpha^T K \alpha.$$

Here,  $\alpha$  and  $C$  are both functions of each  $\theta_i$  and  $\dot{\theta}_i$ , and note that  $C$  is a strictly positive constant with respect to  $\omega$ . In this form, it is clear that the  $\omega$ , which pointwise minimizes the integrand is  $\omega = \alpha$ .

After substituting  $\omega = \alpha$  into (3) to eliminate the first term, we use variational calculus to convert the problem into a set of differential equations. The functions  $\theta_1, \dots, \theta_{n-1}$ , which minimize the functional may be obtained by  $n - 1$  applications of the Euler–Lagrange equation

$$\frac{\partial C}{\partial \theta_i} - \frac{d}{ds} \left( \frac{\partial C}{\partial \dot{\theta}_i} \right) = 0.$$

This yields the following system of coupled nonlinear differential equations (analogous to the main result, derived in frames of minimal rotation, in [9]):

$$(\alpha - \bar{\omega}_i^*)^T K_i \frac{\partial \bar{\omega}_i^*}{\partial \theta_i} - (\dot{\alpha} - \dot{\bar{\omega}}_i^*)^T K_i \frac{\partial \bar{\omega}_i^*}{\partial \dot{\theta}_i} = 0 \quad (4)$$

for  $i \in \{1, \dots, n - 1\}$  with the boundary conditions  $\theta_i(0) = \theta_{i0}$  and  $\dot{\theta}_i(\ell) = 0$ . Solving (4) for the functions  $\theta_i(s)$  and obtaining the final backbone shape of the cannula is the subject of the following section.

### III. SOLVING FOR CANNULA SHAPE

Equation (4) can be reformulated to facilitate numerical integration as follows. We can write it in matrix form as

$$\ddot{\theta} = \mathbf{T}^{-1} \mathbf{f}(\theta, s) + \dot{\tau}(s) \quad (5)$$

where  $\mathbf{T} = [t_{i,j}]$  is an  $(n - 1) \times (n - 1)$  symmetric matrix given by

$$t_{i,j} = \begin{cases} \frac{J_i G_i \sum_{k=1, k \neq i}^n J_k G_k}{\sum_{k=1}^n J_k G_k}, & i = j \\ \frac{-J_i G_i J_j G_j}{\sum_{k=1}^n J_k G_k}, & i \neq j \end{cases}$$

$$\tau(s) = [\tau_1 - \tau_n \quad \tau_2 - \tau_n \quad \dots \quad \tau_{n-1} - \tau_n]^T$$

$$\theta = [\theta_1 \quad \dots \quad \theta_{n-1}]^T$$

$$\mathbf{f}(\theta, s) = [f_1 \quad \dots \quad f_{n-1}]^T,$$

and

$$f_i = \frac{E_i I_i \kappa_i(s) \left( \sum_{k=1, k \neq i}^n E_k I_k \kappa_k(s) \sin(\theta_i - \theta_k) \right)}{\sum_{k=1}^n E_k I_k}.$$

Note that the concise form of (5), which is enabled by the use of the Frenet–Serret apparatus to frame the undeformed tube curves, enables us to interpret this general formulation as an extension of prior models for circular tubes. The vector  $\hat{\tau}(s)$  acts as a forcing function in the general case (5), whereas  $\hat{\tau}(s) \equiv 0$  for circularly precurved tubes ( $\omega_i^* = \kappa_i e_1$ ). Thus, in the case of two circular tubes, (5) reduces to the single differential equation derived in [8]. Indeed, it is evident from (5) that the simple equation in [8] applies not only for two circular tube shapes, but also for any two planar shapes, any two helical shapes, and in general, for any two space curves whose Frenet–Serret torsion is constant. In the case of circular or helical tube shapes, (5) is especially simple, because it is of the form  $\dot{\theta} = f(\theta)$  with no explicit dependence on  $s$ .

To numerically evaluate the general (5), it is useful to put it in the form  $\dot{x} = f(x)$ . To do so, one can augment the vectors on each side of the equation. Let  $x_i = \theta_i$  for  $1 \leq i \leq n-1$ , and let  $x_i = \dot{\theta}_{i-n+1}$  for  $n \leq i \leq 2n-2$ . The augmented first-order system is then

$$\dot{x} = \begin{bmatrix} [x_n, x_{n+1}, \dots, x_{2n-2}]^T \\ \mathbf{T}^{-1} \mathbf{f}(x_1, x_2, \dots, x_{n-1}) \end{bmatrix} + \begin{bmatrix} 0 \\ \hat{\tau} \end{bmatrix}. \quad (6)$$

In this case of fully overlapping tubes of length  $\ell$ , the boundary conditions will be  $x_i(0) = \theta_i(0)$  for  $1 \leq i \leq n-1$  and  $x_i(\ell) = \dot{\theta}_{i-n+1}(\ell) = 0$ , for  $n \leq i \leq 2n-2$ . This system may now be solved numerically with a boundary value algorithm (e.g., collocation, finite difference, or a shooting method). In the simulations in this paper, we use MATLAB's collocation solver `bvp4c`. Computation time depends strongly on the complexity of the problem and the accuracy of the initial guess, but for our unoptimized simulations, it was usually around 0.5 s on a 2.6-GHz PC.

Depending on the parameters, (6) may have multiple solutions. This bifurcation phenomenon has been observed in physical active cannulas and is described in [2]. While the model presented earlier is for a single section of overlapping tubes, it is straightforward to generalize it to an active cannula with multiple regions of overlap where tubes end at different locations. This is accounted for by considering each region of unique tube overlap (between arc length positions where any tube ends) separately, with its own system of differential equations. By enforcing continuity of the boundary conditions across the junctions of these continuous regions, one can construct one large system to describe the entire cannula. The system obtained in this manner will be equivalent to simply considering (5) to be piecewise defined, with  $E_i = 0$  and  $G_i = 0$  for all arc lengths where tube  $i$  is not present, and the boundary conditions to be staggered ( $\dot{\theta}_i(l_i) = 0$ , with  $l_i$  the arc length where the  $i$ th tube ends).

Once one has solved (6) numerically to obtain each  $\theta_i(s)$  and  $\dot{\theta}_i(s)$ , one can use the earlier result  $\omega = \alpha$  to compute  $\omega$ . The final backbone transformation  $g(s) = \{R(s), p(s)\}$  is obtained by solving the differential equation  $[e_3^T \ \omega^T]^T = (g^{-1}(s)\dot{g}(s))^V$ . As reviewed in [14], there exist a number of numerical integration techniques for doing so that preserve the group structure of SE(3). A simple first-order method consists of approximating  $\omega$  by discretizing it and assuming constant values over each segment, then applying the product of exponentials formula, as given in [12].

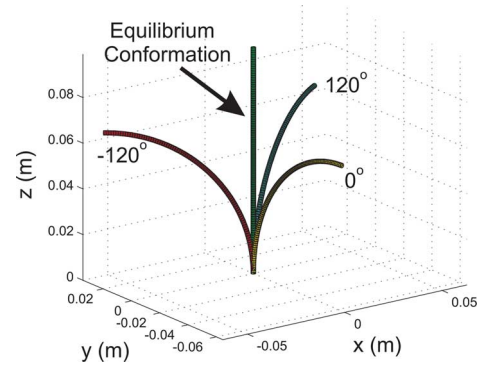


Fig. 2. Equilibrium conformation of three identical 100 mm tubes spaced evenly at  $0^\circ$ ,  $120^\circ$ , and  $-120^\circ$ . The resulting shape is straight.

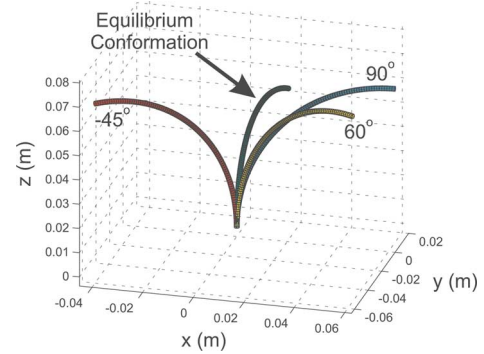


Fig. 3. Equilibrium conformation of three identical 100 mm tubes, rotated to  $60^\circ$ ,  $90^\circ$ , and  $-45^\circ$  is shown to be nonplanar. All three tubes must undergo both bending and torsion in order to reach this conformation.

#### IV. EXAMPLE CASE STUDIES

We now apply the model developed in Sections II and III to compute several cannula conformations. While our modeling framework is applicable to larger numbers of tubes with more complex preset shapes, the illustrative examples selected here were chosen because: 1) their equilibrium conformation is somewhat intuitive and 2) they are largely not possible to consider using prior models. All tubes modeled in these simulations have an OD of 2 mm, an ID of 1 mm, a Young's modulus of 50 GPa, a Poisson's ratio of 0.3, and an arc length of 100 mm. We note that these parameters are similar to those of the physical prototype cannulas used in [2] and [6].

Figs. 2 and 3 show simulations of three combined tubes, each of which is a quarter-circle arc. In Fig. 2, the tubes are rotated to angles of  $0^\circ$ ,  $120^\circ$ , and  $-120^\circ$ . Our model agrees with the intuition that the equilibrium conformation should be a straight cannula along the  $z$ -axis, as shown in the figure. This is a trivial solution of the model differential equation,  $\theta_i(s) = \theta_i(0)$  showing that there is no torsional deformation. Consequently, the torque at tube bases is zero.

Fig. 3 shows these tubes rotated to angles of  $90^\circ$ ,  $60^\circ$ , and  $-45^\circ$ , illustrating a case where all tubes undergo bending and torsion simultaneously. The simulation indicates torques at tube bases of  $-0.36$ ,  $-0.16$ , and  $0.52$  N·m, respectively. The resulting equilibrium conformation lies where intuition would indicate, between the  $60^\circ$  and  $-45^\circ$  tubes, but nearer to the  $60^\circ$  tube. Note

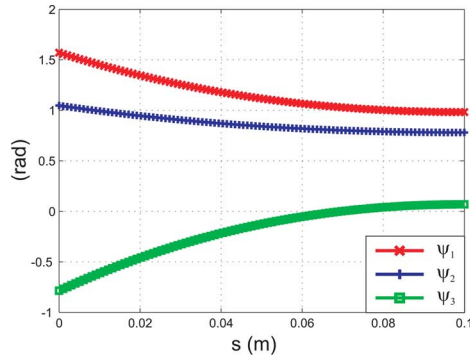


Fig. 4. Axial twist angles (7) for each tube as functions of arc length for the simulation shown in Fig. 3. These “relax” along the arc length, moving toward each other, and their derivatives reach zero at the tube tips.

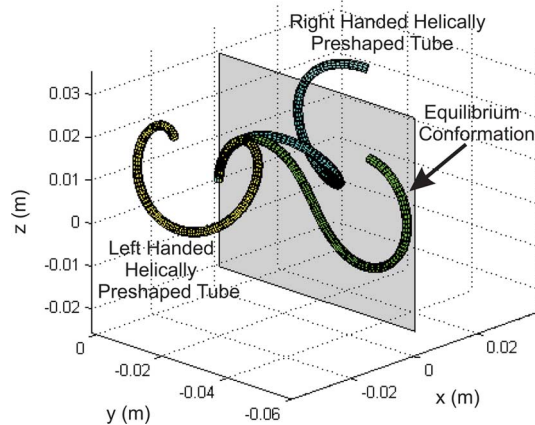


Fig. 5. Two helically shaped 100 mm tubes with equal material properties reach an equilibrium conformation in the plane of symmetry between the two helices.

that the equilibrium conformation is also noncircular, thereby agreeing with the results of [8] and [9].

The amount of torsional deformation that the tubes undergo is given by axial angles  $\psi_i(s)$ , which describe the total axial rotation that has taken place in deformation

$$\psi_i(s) = \psi_i(0) + \int_0^s (\boldsymbol{\omega}_i(\sigma) - \boldsymbol{\omega}_i^*(\sigma))^T \mathbf{e}_3 d\sigma \quad (7)$$

where  $\psi_i(0)$  is the angle to which the base of tube  $i$  is rotated. These angles are plotted in Fig. 4 for the case of the simulation shown in Fig. 3. Note that the angles begin at the base input values, and “relax” along the length of the cannula until their derivatives reach zero at its tip.

In Fig. 5, we simulate two tubes with helical, rather than circular, initial backbone curves. The orientation of the two helices is symmetric about the  $x$ - $z$  plane, so intuition suggests that the equilibrium conformation should lie in that plane, as our model predicts. The simulation indicates base torque magnitudes of 0.61 N·m for each tube. Note that this simulation exhibits multiple solutions as has been seen in prior experiments with physical tubes [2]. In another solution, the tubes rotate the opposite axial

directions to conform to a similarly intuitive, roughly circular shape in the plane of symmetry.

## V. CONCLUSION

In this paper, we have built upon the framework of [2] and [9] by deriving a parsimonious representation and integration method for the differential equations defining active cannula shape. As outlined in Section I, this framework has been developed over time as effects of bending, torsion, and variable precurvature have been sequentially added, leading to predictions that match experiments within a few millimeters [2], [9]. Among the potential future enhancements to the modeling framework are the addition of shear, elongation, frictional effects, and external forcing. The extent to which modeling these effects will be necessary depends upon the medical application. For example, since liver ablation can be successful with relatively large margins, current models are likely sufficient. On the other hand, microsurgical applications such as retinal surgery may require a more detailed model. In nearly all foreseeable applications, the parsimonious formulation and integration method described in this paper will be useful tools for future studies on active cannula design and control.

## REFERENCES

- [1] D. C. Rucker and R. Webster, “Mechanics of bending, torsion, and variable precurvature in multi-tube active cannulas,” in *Proc. IEEE Int. Conf. Robot. Autom.*, Kobe, Japan, 2009, pp. 2533–2537.
- [2] R. J. Webster III, J. M. Romano, and N. J. Cowan, “Mechanics of precurved-tube continuum robots,” *IEEE Trans. Robot.*, vol. 25, no. 1, pp. 67–78, Feb. 2009.
- [3] J. Furusho, T. Katsuragi, T. Kikuchi, T. Suzuki, H. Tanaka, Y. Chiba, and H. Horio, “Curved multi-tube systems for fetal blood sampling and treatments of organs like brain and breast,” *J. Comput. Assist. Radiol. Surg.*, vol. 1, pp. 223–226, 2006.
- [4] M. W. Hannan and I. D. Walker, “Kinematics and the implementation of an elephant’s trunk manipulator and other continuum style robots,” *J. Robot. Syst.*, vol. 20, no. 2, pp. 45–63, 2003.
- [5] M. Loser, “A new robotic system for visually controlled percutaneous interventions under X-ray or CT-fluoroscopy,” Master’s thesis, Albert-Ludwig-Universität, Freiburg, Germany, 2002.
- [6] P. Sears and P. E. Dupont, “A steerable needle technology using curved concentric tubes,” in *Proc. IEEE/RSJ Int. Conf. Intell. Robots Syst.*, 2006, pp. 2850–2856.
- [7] R. J. Webster III, A. M. Okamura, and N. J. Cowan, “Toward active cannulas: Miniature snake-like surgical robots,” in *Proc. IEEE/RSJ Int. Conf. Intell. Robots Syst.*, 2006, pp. 2857–2863.
- [8] D. C. Rucker and R. J. Webster III, “Mechanics-based modeling of bending and torsion in active cannulas,” in *Proc. IEEE RAS/EMBS Int. Conf. Biomed. Robot. Biomechanics*, 2008, pp. 704–709.
- [9] D. C. Rucker, R. J. Webster III, G. S. Chirikjian, and N. J. Cowan, “Equilibrium conformations of concentric-tube continuum robots,” *Int. J. Robot. Res.*, in review.
- [10] I. A. Gravagne, “Design, analysis and experimentation: The fundamentals of continuum robotic manipulators,” Ph.D. dissertation, Clemson Univ., Clemson, SC, 2002.
- [11] S. Kheirbaun and J. H. Maddocks, “Elastic rods, rigid bodies, quaternions and the last quadrature,” *Philos. Trans.: Math., Phys. Eng. Sci.*, vol. 355, no. 1732, pp. 2117–2136, 1997.
- [12] R. M. Murray, Z. Li, and S. S. Sastry, *A Mathematical Introduction to Robotic Manipulation*. Boca Raton, FL: CRC Press, 1994.
- [13] M. Bergou, M. Wardetzky, S. Robinson, B. Audoly, and E. Grinspun, “Discrete elastic rods,” *ACM Trans. Graph.*, vol. 27, no. 3, pp. 34–45, 2008.
- [14] J. Park and W.-K. Chung, “Geometric integration on euclidean group with application to articulated multibody systems,” *IEEE Trans. Robot.*, vol. 21, no. 5, pp. 850–863, Oct. 2005.